

*Letter to the Editor***3D simulations of twisted magnetic flux ropes**S.B.F. Dorch¹, V. Archontis², and Å. Nordlund²¹ The Royal Swedish Academy of Sciences, Stockholm Observatory, 13336 Saltsjöbaden, Sweden² The Niels Bohr Institute for Astronomy, Physics and Geophysics, Juliane Maries Vej 30, 2100 Copenhagen Ø, Denmark

Received 6 April 1999 / Accepted 3 November 1999

Abstract. Several numerical simulations of buoyant 2D and 3D twisted flux ropes have been performed. It is found that the apex region of an anchored 3D flux rope behaves similarly to the simpler case of a 2D horizontal twisted flux tube while the overall structure of such a 3D flux rope develops quite differently. Upon emergence a characteristic S-shape of the magnetic field lines is displayed in agreement with observations in soft X-ray.

Key words: instabilities – magnetic fields – Magnetohydrodynamics (MHD) – Sun: activity – Sun: magnetic fields – Sun: sunspots

1. Introduction

Numerical experiments carried out within the thin flux tube approximation (e.g. Spruit 1981 and Moreno-Insertis 1986) are consistent with the observations of the latitudes of emergence and tilt angles of bipolar magnetic regions on the surface of the Sun (Fan et al. 1994 and Caligari et al. 1995). However, more general numerical simulations, not relying on the assumption that the flux tubes are thin, have shown that cylindrical flux tubes are quickly disrupted by a magnetic Rayleigh-Taylor instability, whereby characteristic “mushroom” structures are created, and the flux tubes lose their buoyancy (Schüssler 1979, Tsinganos 1980, Cattaneo & Hughes 1988, Cattaneo et al. 1990, Matthews et al. 1995, Moreno-Insertis & Emonet 1996, Emonet & Moreno-Insertis 1996, 1998 and Dorch & Nordlund 1998). This is a result of the simple topology assumed for the magnetic field of the flux tubes: A parallel field has no inhibiting effect on the Rayleigh-Taylor instability.

Magnetic field lines may become twisted as a result of the complex mapping of turbulent convective velocity flows, or as a result of rotational shear acting on flux ropes located at the bottom of the convection zone, that connect across the equator. The magnetic field line tension resulting from a twist may suppress the Rayleigh-Taylor instability and hence prevent the flux ropes from disintegrating. This has been demonstrated in nu-

merical 2D simulations (e.g. Emonet & Moreno-Insertis 1996 and 1998). In 3D the presence of a twist means that there is a possibility for the rope to kink. As a twisted buoyant flux rope ascends up through the convection zone, its magnetic field intensity will weaken by several orders of magnitude, because of the expansion of the rope. However, the longitudinal and transverse field components do not decrease in proportion (e.g. Priest 1990 and Kuznetsov & Hood 1997). As first shown by Parker (1974) the transverse component of the magnetic field has a tendency to become concentrated in the expanded portion of a rope. Since the kink instability and other 3D effects such as curvature leading to the Parker-instability, cannot be represented in 2D, numerical 3D simulations are called for.

2. Model

The resistive and compressible MHD-equations, written in conservative form and neglecting rotation (see Dorch & Nordlund 1998), are solved in a Cartesian box using the computational scheme by Galsgaard and others (e.g. Galsgaard & Nordlund 1997 and Nordlund et al. 1994): A finite difference staggered mesh with 6th order derivative operators, 5th order centering operators and a 3rd order Hyman time-stepping routine. In this scheme the viscous and magnetic diffusive terms are quenched in regions with smooth variations, to reduce the diffusion of well-resolved structures. Typical magnetic Reynolds numbers in non-smooth regions are of the order of a few times 10^2 , while in smooth regions it can be substantially higher.

We present results from simulations of flux ropes with an initial entropy balance $\Delta S = 0$ between the interior of the rope and the external medium. This corresponds to buoyancy a factor of γ lower than in the case of temperature balance. Through-out the simulations the buoyancy deviates only slightly from $1/(\gamma\beta)$ (on the average $\sim 3\%$) indicating that ΔS does not change significantly due to artificial diffusion. This type of initial condition was also recently used by Moreno-Insertis & Emonet (1996) and Emonet & Moreno-Insertis (1998) and has the advantage that the relatively high buoyancy results in a significantly shorter run-time than e.g. evolving the flux ropes from an initial perturbed state of mechanical equilibrium. The initial twist of the flux ropes are given by

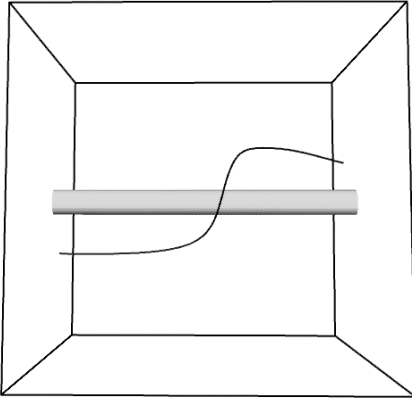


Fig. 1. A snapshot from the 3D simulation of a twisted horizontal flux rope: The rope is seen from “above” at $t = 44$ sound crossing times. Note: Only the central half of the computational box is shown.

$$B_z = B_0 e^{-(r/R)^2}, \quad B_\phi \propto B_z (r/R)^3 e^{-(r/R)^2}, \quad (1)$$

where B_z is the parallel and B_ϕ the transversal component of the magnetic field with respect to the rope’s main axis. B_0 is the amplitude of the field and R the radius. This expression for the twist has been applied in 2D simulations and it has been shown that for these cases the Rayleigh-Taylor instability is inhibited if the degree of twist is sufficiently high (Moreno-Insertis & Emonet 1996 and Emonet & Moreno-Insertis 1996, 1998). This kind of topology is simple but similar to the relaxed state of a flux rope with a more complicated topology (Dorch & Nordlund 1998).

The vertical essentially 1D stratification in the computational box is two-fold consisting of a lower, sub-adiabatically stratified layer and an upper, adiabatically stratified “convection zone”. The purpose of the sub-adiabatic layer is to model the average sub-adiabatic undershoot layer. Both layers are initially in hydrostatic equilibrium and convection is absent during the simulations.

3. Results

We have performed several simulations of buoyant flux ropes in both 2D and 3D, but below we discuss first a 2D and a 3D simulation of a horizontal (straight) twisted flux rope, and then a 3D simulation of an undular twisted flux rope with its feet anchored in the sub-adiabatic layer.

A 2D calculation in a box with 150×100 grid points, and a 3D calculation with $150 \times 100 \times 200$ grid points were performed. The height of the box was $h = \frac{1}{2} H_P$ and the width $L \approx \frac{1}{3} H_P$. In the 3D case, the length of the box and the flux rope was $L \approx \frac{2}{3} H_P$, with H_P being the pressure scale height at the bottom of the box. The rope was not unstable to the Parker-instability (Spruit & van Ballegoijen 1982) since this would require it to be at least an order of magnitude longer.

A radius of $R = 3.7 \times 10^{-2} H_P$ and a plasma beta of $\beta = 10^3$ was chosen to ensure a sufficiently short time of rise. The maximum field line pitch occurs at a radial distance of $\sqrt{3/2}R$ from the rope’s axis. Emonet & Moreno-Insertis (1996) showed

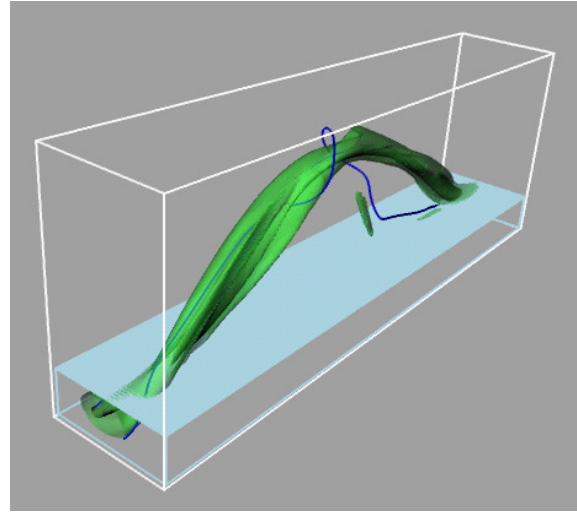


Fig. 2. A snapshot showing the ascending 3D twisted undular flux rope. The feet of the rope are anchored in the stable lower layer. Isosurfaces of magnetic field strength are shown at low field strength (transparent) and at high field strength (opaque). Also shown is a single weak magnetic field line.

that to prevent the Rayleigh-Taylor instability a maximum pitch angle of 10° is needed for this particular twist topology. We set the maximum pitch angle equal to 20° and thus the field lines with the maximum pitch encircle the flux rope main axis only once.

The general result of the 2D simulation was that the Rayleigh-Taylor instability was inhibited and the rope performed oscillations about its center as it rose (see also Emonet & Moreno-Insertis 1998). The maximum pitch angle of the rope increased as the central part of the rope squeezed the rope apex.

The results for the case of a horizontal 3D rope are consistent with the 2D results. As the rope rose the pitch increased until it saturated, as the flux rope entered a quasi-steady regime, where the topology hardly changed during the rise. At that point the field lines just below the stagnation point in front of the rope were virtually perpendicular to the main axis of the rope (see Fig. 1) while the field lines just below the rope were effectively parallel to it.

A 3D simulation of a twisted undular flux rope was performed with $150 \times 80 \times 200$ grid points. The pressure contrast of the adiabatic “convection zone” was 5.1, the height of the box $h = 1.5 H_P$, and the stably stratified lower layer (with $\delta = -1$) had a thickness of $0.3 H_P$.

The wavelength of the sinusoidal flux rope was set to $\lambda = 4.2 H_P$ so that the flux rope was not Parker-unstable even though the stratification admits this instability for ropes longer than the critical wavelength of $12 H_P$ (Spruit & van Ballegoijen 1982). The amplitude of the undulation of the rope was set to $\Delta l = 3.5 \times 10^{-2} \lambda$ and the radius to $R = 5 \times 10^{-2} H_P$. Initially the rope was twisted, with a maximum pitch angle of 30° , well above the Rayleigh-Taylor stability criterion.

Fig. 2 shows a snapshot from a well developed stage: While the part of the rope that is in the adiabatic zone starts to ascend,

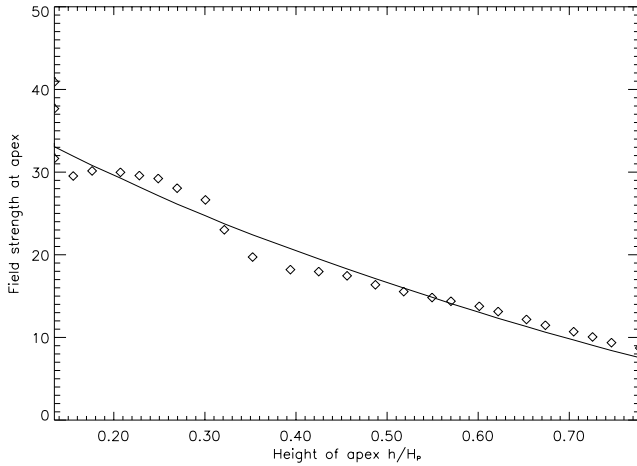


Fig. 3. Field strength at the apex of the rope (symbols) as a function of the apex height above the stable layer. Also shown is the predicted decrease of the magnetic field strength in an adiabatically rising flux rope with a polytropic internal stratification.

the feet remain anchored in the stable layer through-out the simulation, because of the strong sub-adiabatic stratification.

The structure of the magnetic field near the apex of the flux rope is similar to what was obtained for horizontal flux ropes. The weak magnetic field line shown has a very high pitch angle in front of the rope but is almost parallel behind it. The effect of this weak field is the same as in the case of straight but twisted 3D or 2D flux ropes, i.e. it helps to suppress the Rayleigh-Taylor instability, that otherwise threatens to break up the ropes.

After the initial acceleration due to buoyancy, the rope's apex enters a quasi-stationary regime, where its speed approaches a terminal value of 1.5% of the sound speed in an oscillatory manner. In 2D this behavior is a result of the competition between buoyancy and aerodynamic drag (Emonet & Moreno-Insartis 1998), but in 3D the magnetic force associated with the main curvature of the rope, is the primary competitor to buoyancy.

Fig. 3 shows the magnetic field strength at the rope's apex as a function of time. The field decreases almost monotonically although some oscillations are seen. Dorch & Nordlund (1998) showed that the evolution of a 2D flux rope with a complex field topology closely followed the evolution of an adiabatically ascending flux rope with an internally polytropic stratification. The behavior of the apex field fits well with this simple estimate, showing that the weakening of the field strength is mainly due to the decreasing external pressure.

According to Galsgaard & Nordlund (1997) the kink instability in general sets in, when the twist of a magnetic structure is of the order of $4\pi - 8\pi$, depending on various parameters such as diameter and field strength. Another criterion for a twisted flux tube to kink, is that $qR > 1$, where $q = B_\phi / (RB_z)$ is the helical pitch (Linton et al. 1996). Since the initial maximum pitch angle was set to 30° the field lines with the maximum pitch correspond to a twist of the order of 15π along the rope. Initially the value of the maximum pitch of the flux rope was below the criterion by Linton et al. (1996) but above that of Galsgaard & Nordlund (1997). However, in the interior of the flux rope,

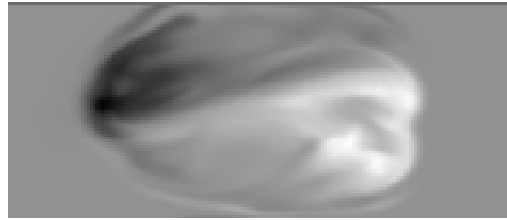


Fig. 4. A snapshot of the vertical component of the magnetic field in a horizontal cross-section of the box as the rope emerges through the open boundary (only half of the box in the direction parallel to the rope is shown).

the pitch angle as given by the expressions Eq. 1 and 2 was significantly smaller than the maximum of 30° . This explains that as a whole, the flux rope has twisted isosurfaces and looks similar to a twisted rubber band (Fig. 2), but does not develop a full-blown kink. For a recent study of kink-unstable flux ropes see e.g. Fan et al. (1998).

Initially the feet, legs, and apex of the rope had the same cross-section, and the rope was symmetric around the apex. These three parts of the rope develop, however, rather differently. The feet perform buoyancy oscillations for a short time only before they are firmly anchored in the lower layer and quite flat. The legs become very elongated in the vertical direction and as they rise they leave behind a considerable amount of their magnetic field in a wake. The behavior and shape of the apex of the rope is similar to that obtained in 2D simulations of twisted buoyant flux tubes; a weak transversal field protects the strongly buoyant more or less parallel core component of the field against the external medium.

As the apex of the flux rope approaches the upper boundary of the box, the open boundary condition begins to influence the evolution of the rope. Fig. 4 shows a horizontal cross section of the magnetic field as the rope emerges through the boundary. A “bipolar region” is formed by the emerging legs and the “spots” separate as the rope rises through the surface. At some stages of the emergence the magnetic field has a characteristic S-shape similar to what is observed in soft X-rays images of magnetic surface structures (see Canfield et al. 1999).

In a recent study Matsumoto et al. (1998) showed that a buoyant flux rope that initially is given a Gold-Hoyle twist (independent of radius) is significantly kink unstable and for the emergence of a twisted flux rope they obtain results similar to the above. It is worth noticing, however, that the difference in initial field line topology may result in large differences in the subsequent overall behavior of the flux ropes: The Gold-Hoyle twist is more likely to give a kink than the case discussed here, because the main twist in the present case is confined to a thin layer around the rope as found in the case of Dorch & Nordlund (1998).

4. Summary and conclusions

The present study confirms that some degree of twist of the magnetic field lines is needed to prevent a break-up of flux structures

in a magnetic Rayleigh-Taylor instability because of differential buoyancy and the interaction with the external stratification. The 2D work of Dorch & Nordlund (1998) has been extended to cases of 3D twisted horizontal flux ropes, as well as to 3D twisted undular flux ropes. The studies of 3D twisted horizontal flux ropes are in complete agreement with the corresponding 2D studies (as they should be) but the 3D simulations of twisted undular flux ropes deviates in important respects from the 2D simulations.

Magnetic tension is present in topologically complex fields such as fields generated by turbulent motions producing a chaotic mapping of field lines. It is likely that the dynamo generated field stored in the undershoot layer has such a complex topology. The origin of a net-twist such as the one assumed above is non-trivial. It might be a consequence of the radial shear in the undershoot layer, acting on flux structures connected across the equator, but this has not yet been proven.

A lot of dynamically important effects have not been included in the present discussion, e.g. in the case of the 3D flux rope the apex rises only about one pressure scale height, and therefore the radius of the rope is still not large compared to the external adiabatic stratification. The expansion of flux ropes as they rise to lower pressures than has been modeled here will probably have strong effects on the stability of the ropes.

The main results from numerical 2D simulations of buoyant horizontal flux tubes hold to a good approximation for the apex of 3D flux ropes: The suppression of the Rayleigh-Taylor instability by transversal field lines due to a twist of the rope, oscillations of the apex as it rises, the shape of a cross section of the rope apex, the generation of vortex rolls, and the decrease of the magnetic field at the apex are all phenomena that are similar to what is found in the 2D case. The main differences are that in the 3D case in addition to drag, magnetic tension towards the radius of curvature of the undular rope is present and may further reduce the ascent velocity, and that the behavior of the legs and feet of the rope cannot be correctly modeled in 2D. The shape and behavior of the emerging “bipolar region” that is formed when the rope emerges through the surface is in general agreement with the observations in e.g. soft X-ray of S-shaped active regions (by e.g. the Yohkoh satellite).

In the real solar convection zone buoyant flux structures are constantly interacting with the surrounding turbulent convec-

tion, convective downdrafts and updrafts, and neighboring flux structures. The question remains whether the quasi-steady state topology that the flux ropes reach in the later phase of their rise is stable towards perturbations from the surroundings, and whether the results reported here, for 3D flux ropes moving in a 1D static stratification, at all carry over to the more realistic case. Simulations of 3D flux ropes ascending in a dynamic 3D convection zone are under way.

Acknowledgements. Computing time at the UNI●C computing center was provided by the Danish Natural Science Research Council. SBF D acknowledges support through an EC-TMR grant to the European Solar Magnetometry Network.

References

- Canfield, R.C., Hudson, H.S., and McKenzie, D.E., 1999, *Geoph. Res. Letters* 26(6), 627
- Caligari, P., Moreno-Insertis, F., and Schüssler, M., 1995, *ApJ* 441, 886
- Cattaneo, F., Chiueh, T., and Hughes, D., 1990, *JFM* 219, 1
- Cattaneo, F. and Hughes, D., 1988, *JFM* 196, 323
- Dorch, S.B.F. and Nordlund, Å., 1998, *A&A* 338, 329
- Emonet, T. and Moreno-Insertis, F., 1996, *ApJ* 458, 783
- Emonet, T. and Moreno-Insertis, F., 1998, *ApJ* 492, 804
- Fan, Y., Fisher, G.H., and DeLuca, E.E., 1993, *ApJ* 405, 390
- Fan, Y., Fisher, G.H., and McClymont, A.N., 1994, *ApJ* 436, 907
- Fan, Y., Zweibel, E.G., Linton, M.G., and Fisher, G.H., 1998, *ApJ* 505, L59
- Galsgaard, K. and Nordlund, Å., 1997, *Journ. Geoph. Res.* 102, 219
- Kuznetsov, V. and Hood, A., 1997, *Solar Physics* 171, 61
- Linton, M., Longcope, D., and Fisher, G., 1996, *ApJ* 469, 954
- Matsumoto, R., Tajima, T., Chou, W., Okubo, A., and Shibata, K., 1998, *ApJ* 493, L43
- Matthews, P., Hughes, D., and Proctor, M.R.E., 1995, *ApJ* 448, 938
- Moreno-Insertis, F., 1986, *A&A* 166, 291
- Moreno-Insertis, F. and Emonet, T., 1996, *ApJ* 472, L53
- Nordlund, Å., Galsgaard, K., Stein, R.F., 1994, in *Solar Surface Magnetic Fields* 433, NATO ASI Series,
- Parker, E.N., 1974, *ApJ* 191, 245
- Priest, E.R., 1990, in *Physics of magnetic flux ropes*, 1
- Schüssler, M., 1979, *A&A* 71, 79
- Spruit, H.C., 1981, *A&A* 98, 155
- Spruit, H.C. and van Ballegoijen, A.A., 1982, *A&A* 106, 58
- Tsinganos, K., 1980, *ApJ* 239, 746